BBA - Biomembranes 1861 (2019) 1421–1427

Contents lists available at ScienceDirect

BBA - Biomembranes

journal homepage: www.elsevier.com/locate/bbamem

The distal cytoplasmic tail of the influenza A M2 protein dynamically extends from the membrane

Grace Kim[1], Hayley E. Raymond[1], Alice L. Herneisen[2], Abigail Wong-Rolle, Kathleen P. Howard*

Department of Chemistry and Biochemistry, Swarthmore College, Swarthmore, PA 19081, United States of America

ARTICLE INFO

Keywords:
Full-length influenza A M2 protein
Cytoplasmic tail
Site-directed spin labeling
Electron paramagnetic resonance

ABSTRACT

The influenza A M2 protein is a multifunctional membrane-associated homotetramer that orchestrates several essential events in the viral infection cycle. The monomeric subunits of the M2 homotetramer consist of an N-terminal ectodomain, a transmembrane domain, and a C-terminal cytoplasmic domain. The transmembrane domain forms a four-helix proton channel that promotes uncoating of virions upon host cell entry. The membrane-proximal region of the C-terminal domain forms a surface-associated amphipathic helix necessary for viral budding. The structure of the remaining ~34 residues of the distal cytoplasmic tail has yet to be fully characterized despite the functional significance of this region for influenza infectivity. Here, we extend structural and dynamic studies of the poorly characterized M2 cytoplasmic tail. We used SDSL-EPR to collect site-specific information on the mobility, solvent accessibility, and conformational properties of residues 61–70 of the full-length, cell-expressed M2 protein reconstituted into liposomes. Our analysis is consistent with the predominant population of the C-terminal tail dynamically extending away from the membranes surface into the aqueous medium. These findings provide insight into the hypothesis that the C-terminal domain serves as a sensor that regulates how M2 protein participates in critical events in the viral infection cycle.

1. Introduction

The influenza A virus causes seasonal epidemics and global pandemics, thereby posing a critical public health risk [1]. An atomic-level understanding of each step of the viral life cycle could inform new antiviral strategies. The influenza A M2 protein is a multifunctional membrane-associated homotetramer that orchestrates several essential events in the viral infection cycle, such as viral assembly and budding [2,3]. Here, we extend structural and dynamic studies of the poorly characterized M2 cytoplasmic tail.

The 97-residue monomeric subunits of the M2 homotetramer consist of an N-terminal ectodomain, a transmembrane domain, and a C-terminal cytoplasmic domain (Fig. 2A). The transmembrane domain forms a four-helix proton channel that promotes uncoating of virions upon host cell entry [2].

The C-terminal domain regulates viral budding and morphology [3], proton-channel activity [4], and viral assembly through interactions with other influenza virus proteins including the matrix protein M1 [5]. The membrane-proximal region of the C-terminal domain forms a surface-associated amphipathic helix. The structure of the remaining ~34 residues of the distal cytoplasmic tail has yet to be fully characterized despite the functional significance of this region for influenza infectivity.

The functional significance of the distal cytoplasmic tail of M2 protein has been elucidated by several lines of inquiry. A series of deletion mutants of the M2 cytoplasmic tail demonstrated the region had a large impact on the assembly of progeny virions [6]. C-terminal truncations led to reduced nucleoprotein incorporation into virions and altered filament formation on virus-infected cells. The interaction of M2 with matrix protein 1 (M1) has been shown to be critical to the viral replication cycle with the putative binding site near residues 71–76 within the M2 cytoplasmic tail [6–10]. Evidence for the complementary roles of the M1 and M2 proteins in virus assembly has been provided by identification of M1 suppressor mutations that complement a lethal

Abbreviations: SDSL-EPR, site-directed spin labeling electron paramagnetic resonance spectroscopy; ssNMR, solid-state NMR; TM, transmembrane; AH, amphipathic helix; POPC, 1-palmitoyl-2-oleoyl-sn-glycero-3-phosphocholine; POPG, 1-palmitoyl-2-oleoyl-sn-glycero-3-phospho-1-rac-glycerol; CW EPR, continuous-wave electron paramagnetic resonance; NiEDDA, nickel (II) ethylenediaminediacetate

* Corresponding author.
E-mail address: khoward1@swarthmore.edu (K.P. Howard).

[1] Contributed equally to this work.

[2] Current Address: Biology Department, MIT.

https://doi.org/10.1016/j.bbamem.2019.05.021
Received 5 February 2019; Received in revised form 24 May 2019; Accepted 28 May 2019
Available online 30 May 2019
0005-2736/ © 2019 Elsevier B.V. All rights reserved.

tyrosine-to-alanine M2 mutation at amino acid 76 [7]. Detailed biophysical work has focused on the ability of the C-terminal amphipathic helix of M2 to induce curvature necessary for viral budding and scission [11–13]. However, it has also been shown that while the amphipathic helix can generate curvature on its own, the full-length M2 protein is more efficient at generating curvature, suggesting the C-terminal tail is acting synergistically with the amphipathic helix to induce membrane curvature [12].

The M2 protein has been studied by a range of biophysical techniques, including X-ray crystallography [14], solution NMR [15], solid-state NMR (ssNMR) [16–18] and site-directed spin label electron paramagnetic resonance (SDSL-EPR) spectroscopy [19–25]. Until recently, the majority of M2 biophysical studies utilized chemically synthesized truncated constructs that omit the functionally significant cytoplasmic tail domain. The most frequently studied constructs include the transmembrane domain peptide (M2TM, residues ~22–46) or the transmembrane domain with the C-terminal amphipathic helix extension (M2TMC, residues ~22–62).

Here, we use SDSL-EPR, a technique exquisitely suited for detecting the mobility and membrane topology of membrane proteins reconstituted into liposomes [26], to collect site-specific information on the mobility, solvent accessibility, and conformational properties of residues 61–70 of the 97-residue full-length, cell-expressed M2 protein. In previous studies of full-length M2, we characterized the multicomponent nature of M2-WT CW line shapes for sites 50–60 in the C-terminal amphipathic helix and established that they arose from an equilibrium involving two different conformational substates of the protein. Line shapes for sites 61–70 also show evidence of a superposition of two states, although the component arising from the highly mobile population dominates the spectra. Compared to the amphipathic helix proximal to the transmembrane domain, the dominant population of the C-terminal tail is more dynamic and has moved away from the membrane surface into the aqueous phase. The ability to measure both mobility and membrane accessibility parameters of specific sites provides insight into where the membrane-associated amphipathic helix ends. The conformational and dynamic properties of the C-terminal tail beyond the amphipathic helix provide valuable conformational insight into a region of M2 protein known to have a critical role in the regulation of viral assembly and budding.

2. Materials and methods

2.1. Sample preparation

Single cysteine substitutions were introduced into a cysteineless background plasmid based on the A/Udorn/72 M2 sequence [27] using site-directed mutagenesis. Expression, purification, and spin labeling were performed according to previously published protocols [22,25].

Protein was reconstituted into 4:1 1-palmitoyl-2-oleoyl-snglycero-3-phosphocholine/-palmitoyl-2-oleoyl-sn-glycero-3-phospho-1-rac-glycerol lipid bilayers as previously described [28]. This membrane system was chosen for its use in in vitro budding assays [29] and previous SDSL-EPR studies of the M2 protein [20–25]. The buffer used for collection of mobility data and oxygen accessibility measurements was 50 mM Tris pH 7.8, 100 mM KCl, and 1 mM EDTA. The buffer for nickel (II) ethylenediaminediacetate (NiEDDA) accessibility studies was 50 mM NiEDDA, 50 mM Tris pH 7.8, and 100 mM KCl buffer. At pH 7.8 the M2 proton channel does not conduct protons and is in the closed state [2].

2.2. EPR spectroscopy and data analysis

Continuous wavelength (CW) EPR spectra were recorded on an X-band Bruker EMX spectrometer equipped with an ER4123S resonator at room temperature. Samples were placed in 0.6 mm internal diameter, 0.9 mm length gas permeable capillary tubes (L&M EPR Supplies, Milwaukee, WI). CW EPR spectra were acquired using 2 mW incident microwave power, 1 G field modulation amplitude at 100 kHz, and 150 G sweep width.

Power saturation experiments were used to probe the membrane depth of residues. Experiments were collected in the presence of two different paramagnetic relaxation agents, O_2 and NiEDDA. Oxygen is a lipophilic species that partitions in a gradient across the membrane, with the highest O_2 concentration at the center of the bilayer. NiEDDA is water-soluble paramagnetic relaxation agent which is used to measure the accessibility of spin-labeled sites to the aqueous phase. Accessibility experiments were collected under three conditions: equilibrated with ambient air, equilibrated with nitrogen gas, and equilibrated with nitrogen in the presence of NiEDDA. Nitrogen power saturation experiments were collected over 8 power levels. All other power saturation experiments were measured over at least 16 power levels. Data were fit to obtain $\Delta P_{1/2}$ parameters as described previously [20]. Sites with very high accessibility to NiEDDA were not saturated at the powers obtainable. Thus, $\Delta P_{1/2}$(NiEDDA) values greater than 200 should be considered estimates. The contrast parameter, ϕ, was calculated according to the following equation [30]:

$$\phi = \ln\left(\frac{\Delta P_{\frac{1}{2}}(O_2)}{\Delta P_{\frac{1}{2}}(\mathrm{NiEDDA})}\right)$$

3. Results

3.1. Dominant population of the C-terminal tail is highly dynamic beyond the amphipathic helix

The EPR spectral line shapes of spin-labeled residues provide insight into conformational dynamics that reflect both backbone motion as well as secondary and tertiary contacts [26]. EPR line shapes for residues 61–70 are shown in Fig. 1. For comparison, previously reported CW line shapes for sites 50–60 [22] are shown to highlight the marked change in line shapes past the residues closest to the end of the transmembrane domain.

The line shapes for amphipathic helix residues 50–61 are distinctly broader than 62–70. The 50–61 spectra are a superposition of a broad, immobilized component (i), and a sharper, mobile component (m). In previous studies of M2, we characterized the multicomponent nature of the C-terminal amphipathic helix using both line shape analysis and saturation recovery methods to establish the presence of an equilibrium involving two different conformational substates of the protein. We hypothesized that this conformational exchange is relevant for M2 scission function at the edge of the viral budozone [24,25].

Similar to sites 50–61, line shapes for sites 62–70 show evidence of a superposition of two states, although the component arising from a mobile population dominates the spectra. The dynamics of a spin-labeled site can be qualitatively assessed using a semi-empirical mobility factor calculated from the inverse peak-to-peak width of the central line ($\Delta H_0{}^{-1}$) of the EPR line shapes [26]. Mobility factors were calculated from the CW-EPR spectra of each site. In the case of multicomponent spectra, the mobility factors reflect the properties of the overlapping components and provide only a qualitative measure of average dynamics at the site. Nonetheless, mobility factors along a stretch of neighboring residues can provide useful insight into changes in dynamic properties in a specific region of the protein. Mobility as a function of M2 sequence position is shown in Fig. 2B with previously reported data for sites 50–60 for comparison [22]. The mobility of sites 50–61 is low, consistent with restrictions in motion arising from a membrane surface-associated secondary structural element. Mobility factors in the range of 0.2–0.4 have been reported for spin labeled sites within α-helical secondary structure elements within membrane associated proteins [31,32]. In marked contrast to 50–61, spin labels at positions 62–70 exhibit increased mobility.

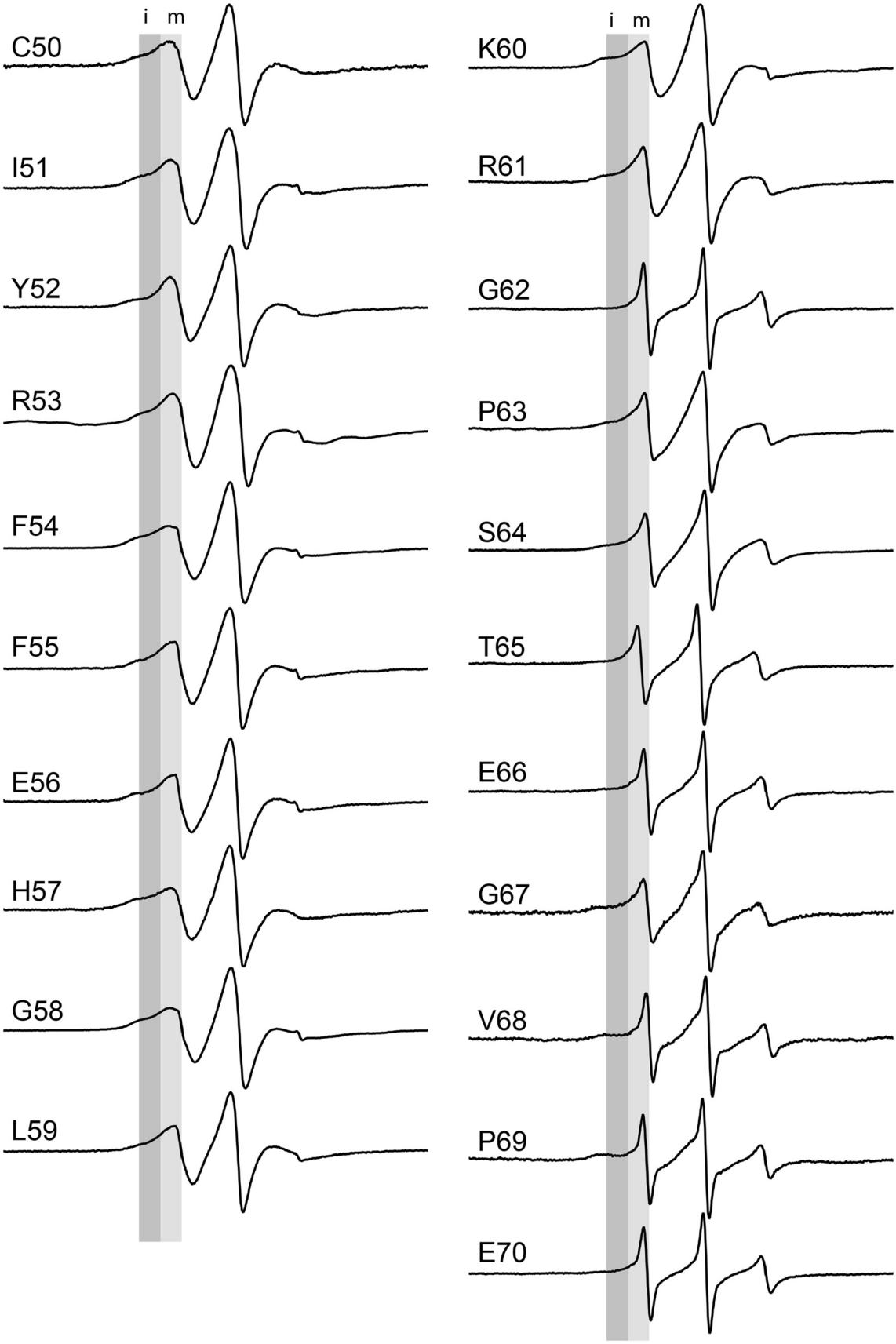

Fig. 1. CW X-band EPR spectra of full-length M2 protein for the indicated sites. Sites 50–60 were reported previously [22] and are part of the surface associated amphipathic helix. Light gray shading highlights mobile (m) peak components. Dark gray shading highlights immobile (i) peak components.

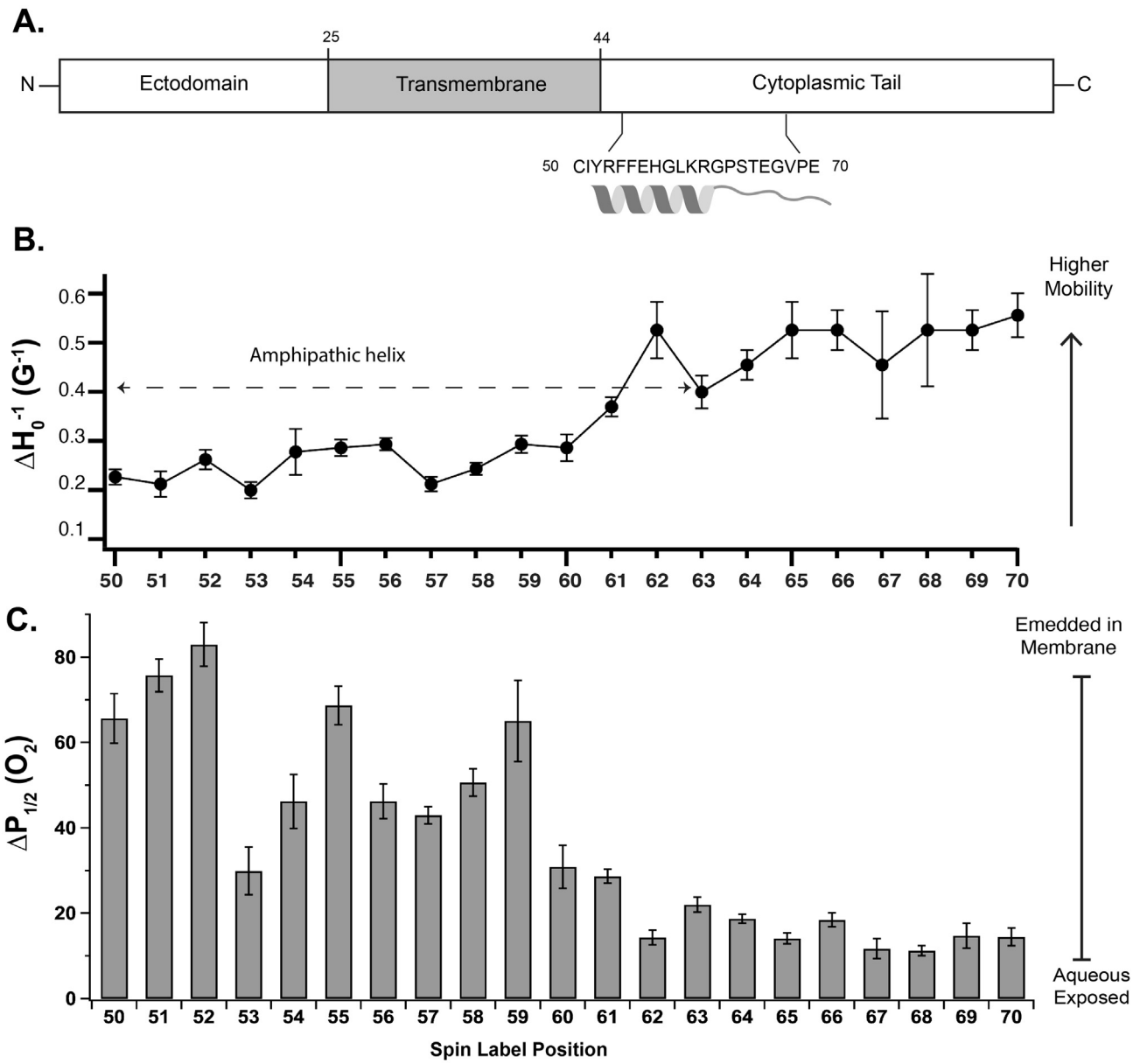

Fig. 2. A. The domain structure of the full-length 97-residue M2 protein. **B**. The relative mobility (inverse central line width, ΔH_0^{-1}) as a function of spin label position. The mobility factors were calculated from CW-EPR spectra shown in Fig. 1. Sites 50–60 were previously published [22] and are included for comparison. Error bars represent the uncertainty in the position of the peak maxima and minima. **C**. Accessibility to oxygen measured by power saturation EPR as a function of spin label position. Error bars represent the 95% confidence intervals from the fits to the power saturation curves.

3.2. The dominant population of the C-terminal tail extends away from the membrane surface

Spin label motional restriction can arise from secondary and tertiary contacts or association with the membrane [26]. Previously, we established that residues 50–60 of the full-length M2 protein form an amphipathic helix associated with the membrane surface. Here, we tested the hypothesis that the observed increase in mobility for sites 62–70 could be attributed to a loss of association with the membrane surface.

We conducted power saturation experiments to measure accessibility to the paramagnetic relaxation agent O_2 which reports on structural topology with respect to the membrane. Oxygen is a lipophilic species that partitions in a gradient across the membrane, with the highest O_2 concentration at the center of the bilayer. The collision rate of the spin label with O_2, quantified by $\Delta P_{1/2}(O_2)$, serves as a relative measurement of membrane accessibility [26].

Oxygen accessibility as a function of spin-label position for sites 61–70 is presented in Fig. 2C along with previously published data for 50–60 for comparison [22]. The overall trend is one of decreasing oxygen accessibility towards the distal cytoplasmic tail, a hallmark of increasing distance from the membrane.

3.3. Conformational properties of the C-terminal tail beyond the amphipathic helix

While O_2 accessibility provides information about the depth of a particular site in the membrane environment, $\Delta P_{1/2}(O_2)$ data can be difficult to interpret for residues positioned near the lipid head groups or in the aqueous environment. To better characterize sites along the membrane-aqueous interface, we employed a water-soluble paramagnetic relaxation agent, NiEDDA, which is used to measure the accessibility of spin-labeled sites to the aqueous phase [26]. Hydrophobic O_2 and hydrophilic NiEDDA have opposite membrane partitioning

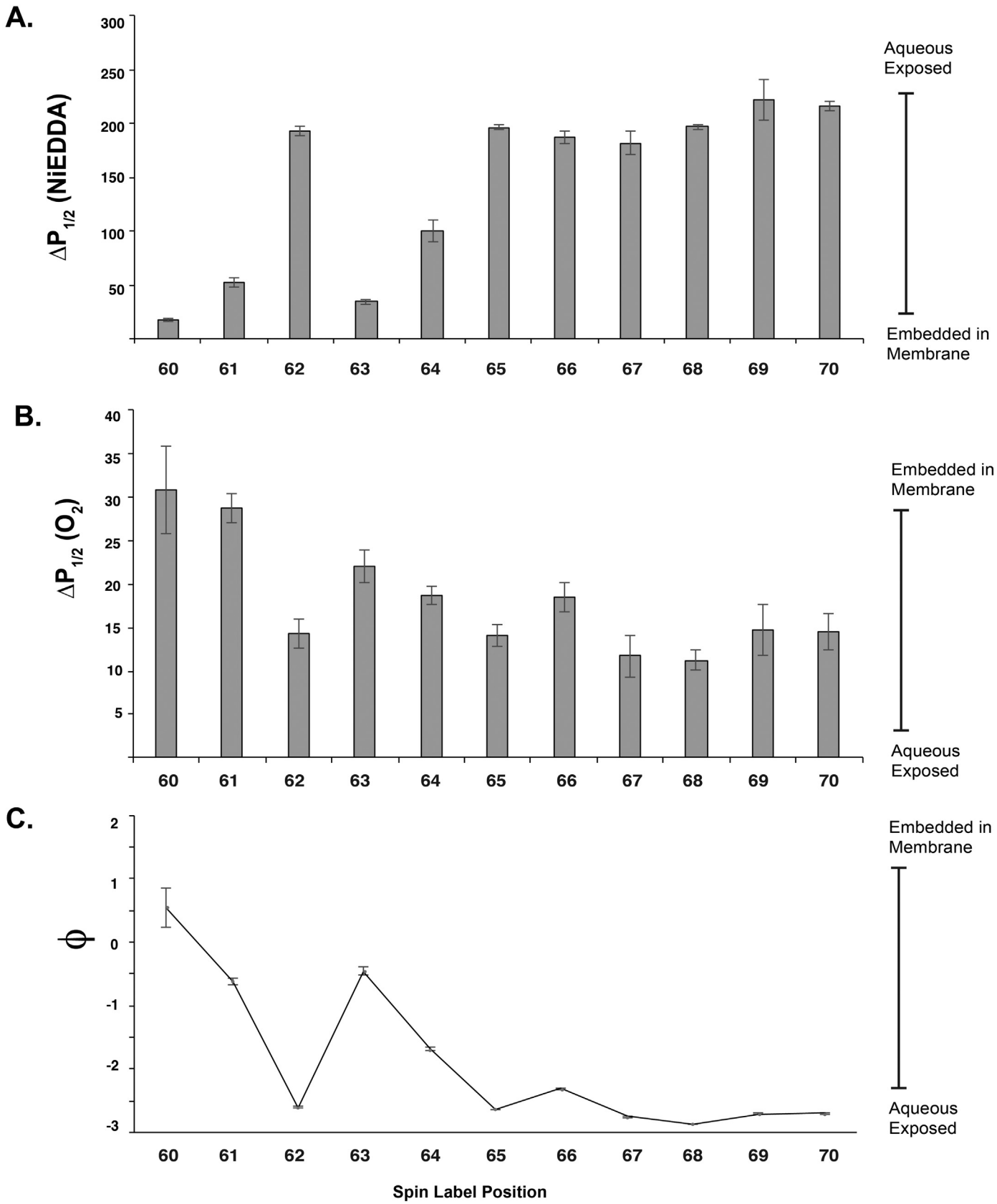

Fig. 3. A. Accessibility to NiEDDA and **B**. O_2 as a function of spin label position for sites 60–70. Representative raw data for O_2 and NiEDDA accessibility measurements shown in Fig. S1. Error bars represent the 95% confidence intervals from the fits to the power saturation curves. **C**. Contrast parameter, ϕ, calculated as described in the Materials and Methods.

tendencies. Consistent with these partitioning tendencies, there is a general trend of increasing NiEDDA accessibility between sites 60 and 70 (Fig. 3A), while the trend is one of decreasing oxygen accessibility (Fig. 3B).

Oscillations in O_2 and NiEDDA accessibilities have been shown to be indicators of secondary structural elements [26]. Residue-by-residue patterns in accessibility to O_2 and NiEDDA can provide a topological map of secondary structure with respect to the membrane [26]. Previous analysis of positions 50–60 in full-length M2 identified a sinusoidal variation in oxygen accessibility with a periodicity of 3.6, characteristic of a surface-associated α-helix [22]. As a general trend, we observed that the NiEDDA and O_2 accessibilities of sites 60–63 oscillate 180° out of phase (Fig. 3A and B). Previous work has demonstrated that presence of secondary structure can be usefully predicted by the calculation of a contrast parameter, ϕ, that combines accessibilities of O_2 and NiEDDA for a given site [30]. Membrane-buried sites display spikes in ϕ values, whereas regions that are homogenously solvated in the aqueous phase exhibit relatively constant ϕ values [30]. As shown in Fig. 3C, the contrast parameters for sites 60–64 oscillate as expected for an amphipathic helix and have magnitudes comparable to those reported for other membrane-associated proteins [33,34]. The contrast parameters for sites 65–70 exhibit little variation. Together with the mobility parameters of these residues (Fig. 2B), the EPR data suggest that sites 65–70 form a dynamic and predominantly disordered region that extends away from the membrane into the aqueous medium. Due to the existence of two components in the line shapes shown in Fig. 1 we are unable to discount the existence of a minor population of ordered secondary structure for 65-70 that is not apparent in the contrast parameters.

4. Discussion

Until recently, the majority of biophysical studies on the M2 protein from influenza A have focused on the transmembrane domain and the C-terminal amphipathic helix extension using chemically synthesized truncated constructs. The contribution of this paper is to provide information on the distal cytoplasmic tail in full-length M2 protein reconstituted in liposomes.

SDSL-EPR line shapes for the distal cytoplasmic tail provide evidence for two conformations. The predominate population is highly dynamic and extends away from the membrane surface. The site-specific resolution of EPR mobility and membrane accessibility data provides insight into where the amphipathic helix ends. The oscillatory pattern in accessibility data suggests the amphipathic helix extends out to residue 64. The EPR data agree with the literature on amino acid sequences typically found at the end of helical regions. The pattern of a glycine followed by a proline (found in 62–63 in the M2 sequence studied here) is a common component of capping motifs prevalent in the C-termini of alpha helices [35].

Our finding that the region beyond the amphipathic region is highly mobile is consistent with earlier ssNMR work [36,37]. A study using chemical shift simulation proposed that unassigned ssNMR peaks from full-length M2 protein arose from an unstructured cytoplasmic tail [36]. A follow-up study on a chemically synthesized truncation, M2(22–71), concluded that the post-amphipathic helix cytoplasmic tail up to residue 71 was disordered and highly dynamic [37]. Our SDSL-EPR approach offers advantages over the previously published work on the C-terminal tail of M2. We use the full-length 97-residue M2 protein that includes the entire cytoplasmic tail, whereas the other study that offers site-specific data [20] utilized a truncated construct, M2 (22–71). Furthermore, we collected data at a 1:500 peptide:lipid ratio, in contrast to the high peptide:lipid ratios (~1:20) required for ssNMR studies, which can complicate the interpretation of data due to potential intermolecular interactions.

It has been hypothesized that the C-terminal tail of M2 helps regulate the multiple roles M2 plays in the influenza viral life cycle [12,38]. The M2 protein is embedded in membrane environments that differ in content depending on the stage of the infection cycle. For example, the influenza virus envelope is enriched in cholesterol compared to the host-cell membrane where M2 facilitates viral budding [3]. Biophysical studies have shown that the conformation and dynamics of the C-terminal domain of M2 differ depending on the membrane context [25,36]. The dynamic cytoplasmic tail may serve as a sensor of changes in membrane composition, as well as the presence of other viral proteins, [36].

Matrix protein 1 (M1) has been proposed to interact with the C-terminal tail of M2 as part of incorporation of the nucleoprotein complex into virions and formation of virions on virus-infected cells. It has been hypothesized that a coil-to-helix conformational change in the C-terminal tail of M2 in the presence of M1 protein might facilitate the M1-M2 interaction [37]. The two-component EPR line shapes reported here support the hypothesis that M2 can populate different conformational states. The predominant population of the C-terminal tail, under the sample conditions used here, dynamically extends away from the membrane surface into the aqueous medium. The minor population we see here could be the state primarily populated in the presence of M1 protein. The hypothesis that the M2 protein has multiple low-energy conformational states is not new [24,39,40]. It has been suggested that the various structural models proposed to date provide snapshots of distinct conformational states sampled by the protein during the viral life cycle [19,23]. The M2 protein has at least two functions: the proton channel activity crucial for uncoating of virions [2] and the formation of virions on virus-infected cells [3]. The different functions of M2 could conceivably require different conformations. Ongoing conformational studies under conditions relevant to viral budding and in the presence of M1 protein will further inform how the C-terminal tail of the M2 protein participates in the viral lifecycle.

5. Conclusions

Until recently, the majority of M2 biophysical studies utilized truncated constructs that omit the functionally significant cytoplasmic tail. The contribution of this paper is to provide information on the cytoplasmic tail in full-length M2 protein. We used SDSL-EPR to collect site-specific information on the mobility, solvent accessibility, and conformational properties of residues 61–70 of the full-length 97-residue M2 protein reconstituted into liposomes. Compared to the amphipathic helix proximal to the transmembrane domain, the dominant population of the distal cytoplasmic tail is more dynamic and has moved away from the membrane surface into the aqueous phase. Evidence for multiple conformations of the C-terminal tail is consistent with previous studies that demonstrate that M2 can populate different conformations [24,39,40]. The C-terminal cytoplasmic tail could be a sensor of changes in both membrane composition and binding of other viral proteins, thus regulating the multiple essential roles M2 plays in the influenza infection cycle.

Funding

This work was supported by NIH grant AI117657-01 to KPH.

Transparency document

The Transparency document associated with this article can be found, in online version.

Appendix A. Supplementary Information

Supplementary data to this article can be found online at https://doi.org/10.1016/j.bbamem.2019.05.021.

References

[1] V.N. Petrova, C.A. Russell, The evolution of seasonal influenza viruses, Nat. Rev. Microbiol. (2018) 47–60.
[2] L.H. Pinto, R.A. Lamb, The M2 proton channels of influenza A and B viruses, J. Biol. Chem. 281 (2006) 8997–9000.
[3] J.S. Rossman, R.A. Lamb, Influenza virus assembly and budding, Virology 411 (2011) 229–236.
[4] S.Y. Liao, Y. Yang, D. Tietze, M. Hong, The influenza M2 cytoplasmic tail changes the proton-exchange equilibria and the backbone conformation of the transmembrane histidine residue to facilitate proton conduction, J. Am. Chem. Soc. 137 (2015) 6067–6077.
[5] M.F. McCown, A. Pekosz, Distinct domains of the influenza A virus M2 protein cytoplasmic tail mediate binding to the M1 protein and facilitate infectious virus production, J. Virol. 80 (2006) 8178–8189.
[6] K. Iwatsuki-Horimoto, T. Horimoto, T. Noda, M. Kiso, J. Maeda, S. Watanabe, Y. Muramoto, K. Fujii, Y. Kawaoka, The cytoplasmic tail of the influenza A virus M2 protein plays a role in viral assembly, J. Virol. 80 (2006) 5233–5240.
[7] H. Liu, M.L. Grantham, A. Pekosz, Mutations in the influenza A virus M1 protein enhance virus budding to complement lethal mutations in the M2 cytoplasmic tail, J. Virol. 92 (2018) 1–14.
[8] B.J. Chen, G.P. Leser, D. Jackson, R.A. Lamb, The influenza virus M2 protein cytoplasmic tail interacts with the M1 protein and influences virus assembly at the site of virus budding, J. Virol. 82 (2008) 10059–10070.
[9] S.L. Zebedee, R. a Lamb, Growth restriction of influenza A virus by M2 protein antibody is genetically linked to the M1 protein, Proc. Natl. Acad. Sci., **86** (1989) 1061–1065.
[10] M.F. McCown, A. Pekosz, The influenza A virus M 2 cytoplasmic tail is required for infectious virus production and efficient genome packaging, J. Virol. 79 (2005) 3595–3605.
[11] K.L. Roberts, G.P. Leser, C.L. Ma, R.A. Lamb, The amphipathic helix of influenza A virus M2 protein is required for filamentous bud formation and scission of filamentous and spherical particles, J. Virol. 87 (2013) 9973–9982.
[12] N.W. Schmidt, A. Mishra, J. Wang, W.F. Degrado, G.C.L. Wong, Influenza virus A M2 protein generates negative Gaussian membrane curvature necessary for budding and scission, J. Am. Chem. Soc. 135 (2013) 13710–13719.
[13] A. Martyna, B. Bahsoun, M.D. Badham, S. Srinivasan, M.J. Howard, J.S. Rossman, Membrane remodeling by the M2 amphipathic helix drives influenza virus membrane scission, Sci. Rep. 7 (2017) 44695.
[14] J.L. Thomaston, M. Alfonso-Prieto, R.A. Woldeyes, J.S. Fraser, M.L. Klein, G. Fiorin, W.F. DeGrado, High-resolution structures of the M2 channel from influenza A virus reveal dynamic pathways for proton stabilization and transduction, Proc. Natl. Acad. Sci. 112 (2015) 14260–14265.
[15] J.K. Claridge, J. Aittoniemi, D.M. Cooper, J.R. Schnell, Isotropic bicelles stabilize the juxtamembrane region of the influenza M2 protein for solution NMR studies, Biochemistry 52 (2013) 8420–8429.
[16] M. Sharma, M. Yi, H. Dong, H. Qin, E. Peterson, D.D. Busath, H.-X. Zhou, T.A. Cross, Insight into the mechanism of the influenza A proton channel from a structure in a lipid bilayer, Science 330 (2010) 509–512.
[17] S.D. Cady, J. Wang, Y. Wu, W.F. DeGrado, M. Hong, Specific binding of adamantane drugs and direction of their polar amines in the pore of the influenza M2 transmembrane domain in lipid bilayers and dodecylphosphocholine micelles determined by NMR spectroscopy, J. Am. Chem. Soc. 133 (2011) 4274–4284.
[18] L.B. Andreas, M.T. Eddy, R.M. Pielak, J. Chou, R.G. Griffin, Magic angle spinning NMR investigation of influenza A $M2_{18-60}$: support for an allosteric mechanism of inhibition, J. Am. Chem. Soc. 132 (2010) 10958–10960.
[19] K.C. Duong-Ly, V. Nanda, W.F. Degrado, K.P. Howard, W.F. Degrad, K.P. Howard, W.F. Degrado, K.P. Howard, The conformation of the pore region of the M2 proton channel depends on lipid bilayer environment, Protein Sci. 14 (2005) 856–861.
[20] P.A. Nguyen, C.S. Soto, A. Polishchuk, G.A. Caputo, C.D. Tatko, C.L. Ma, Y. Ohigashi, L.H. Pinto, W.F. DeGrado, K.P. Howard, pH-induced conformational change of the influenza M2 protein C-terminal domain, Biochemistry 47 (2008) 9934–9936.
[21] J.L. Thomaston, P.A. Nguyen, E.C. Brown, M.A. Upshur, J. Wang, W.F. DeGrado, K.P. Howard, Detection of drug-induced conformational change of a transmembrane protein in lipid bilayers using site-directed spin labeling, Protein Sci. 22 (2013) 65–73.
[22] S. Huang, B. Green, M. Thompson, R. Chen, J. Thomaston, W.F. DeGrado, K.P. Howard, C-terminal juxtamembrane region of full-length M2 protein forms a membrane surface associated amphipathic helix, Protein. Sci. 24 (2015) 405–411.
[23] K. Saotome, K.C. Duong-Ly, K.P. Howard, Influenza A M2 protein conformation depends on choice of model membrane, Pept. Sci. 104 (2015) 405–411.
[24] S.S. Kim, M.A. Upshur, K. Saotome, I.D. Sahu, R.M. McCarrick, J.B. Feix, G.A. Lorigan, K.P. Howard, Cholesterol-dependent conformational exchange of the C-terminal domain of the influenza A M2 protein, Biochemistry 54 (2015) 7157–7167.
[25] A.L. Herneisen, I.D. Sahu, R.M. McCarrick, J.B. Feix, G.A. Lorigan, K.P. Howard, A budding-defective M2 mutant exhibits reduced membrane interaction, insensitivity to cholesterol, and perturbed Interdomain coupling, Biochemistry 56 (2017) 5955–5963.
[26] C.S. Klug, J.B. Feix, Methods and applications of site-directed spin labeling EPR spectroscopy, Methods Cell Biol. 84 (2008) 617–658.
[27] T. Leiding, J. Wang, J. Martinsson, W.F. DeGrado, S.P. Arskold, Proton and cation transport activity of the M2 proton channel from influenza A virus, Proc. Natl. Acad. Sci. U. S. A. 107 (2010) 15409–15414.
[28] C. Crouch, M. Bost, T. Kim, B. Green, D. Arbuckle, C. Grossman, K. Howard, Optimization of detergent-mediated reconstitution of influenza A M2 protein into proteoliposomes, Membranes 8 (2018) 103 1–12.
[29] J.S. Rossman, X.H. Jing, G.P. Leser, R.A. Lamb, Influenza virus M2 protein mediates ESCRT-independent membrane scission, Cell 142 (2010) 902–913.
[30] J.M. Isas, R. Langen, H.T. Haigler, W.L. Hubbell, Structure and dynamics of a helical hairpin and loop region in annexin 12: a site-directed spin labeling study, Biochemistry 41 (2002) 1464–1473.
[31] J. Voss, M.M. He, W.L. Hubbell, H.R. Kaback, Site-Directed Spin Labeling Demonstrates That Transmembrane Domain XII in the Lactose Permease of Escherichia coli Is an α -Helix †, Biochemistry 35 (1996) 12915–12918.
[32] A. Barnakov, C. Altenbach, L. Barnakova, W.L. Hubbell, G.L. Hazelbauer, Site-directed spin labeling of a bacterial chemoreceptor reveals a dynamic, loosely packed transmembrane domain, Protein Sci. 11 (2002) 1272–1481.
[33] A.L. Turner, O. Braide, F.D. Mills, G.E. Fanucci, J.R. Long, Biochimica et biophysica acta residue specific partitioning of KL 4 into phospholipid bilayers, BBA - Biomembranes 1838 (2014) 3212–3219.
[34] C. Altenbach, D.A. Greenhalgh, H.G. Khorana, W.L. Hubbell, A collision gradient-method to determine the immersion depth of nitroxides in lipid bilayers - application to spin-labeled mutants of bacteriorhodopsin, Proc. Natl. Acad. Sci. U. S. A. 91 (1994) 1667–1671.
[35] R. Aurora, R. Srinivasan, G.D. Rose, Rules for α-helix termination by glycine, Science 264 (1994) 1126–1130.
[36] S.Y. Liao, K.J. Fritzsching, M. Hong, Conformational analysis of the full-length M2 protein of the influenza A virus using solid-state NMR, Protein Sci. 22 (2013) 1623–1638.
[37] B. Kwon, D. Tietze, P.B. White, S.Y. Liao, M. Hong, Chemical ligation of the influenza M2 protein for solid-state NMR characterization of the cytoplasmic domain, Protein Sci. 24 (2015) 1087–1099.
[38] S.Y. Liao, M. Lee, M. Hong, Interplay between membrane curvature and protein conformational equilibrium investigated by solid-state NMR, J. Struct. Biol. 206 (2019) 20–28.
[39] F.H. Hu, W.B. Luo, S.D. Cady, M. Hong, Conformational plasticity of the influenza A M2 transmembrane helix in lipid bilayers under varying pH, drug binding, and membrane thickness, Biochim. Biophys. Acta Biomembr. 1808 (2011) 415–423.
[40] M. Yi, T.A. Cross, H.-X.X. Zhou, Conformational heterogeneity of the M2 proton channel and a structural model for channel activation, Proc. Natl. Acad. Sci. U. S. A. 106 (2009) 13311–13316.